First-principles calculations on Si (220) located 6H–SiC ($10\bar{1}0$) surface with different stacking sites*

He Xiao-Min(贺小敏)[a)†], Chen Zhi-Ming(陈治明)[a)], Pu Hong-Bin(蒲红斌)[a)], Li Lian-Bi(李连碧)[b)], and Huang Lei(黄 磊)[a)]

[a)] *Department of Electronic Engineering, Xi'an University of Technology, Xi'an* 710048, *China*
[b)] *School of Science, Xi'an Polytechnic University, Xi'an* 710048, *China*

(Received 12 December 2013; revised manuscript received 11 April 2014; published online 20 August 2014)

6H–SiC ($10\bar{1}0$) surface and Si (220)/6H–SiC ($10\bar{1}0$) interface with different stacking sites are investigated using first-principles calculations. Surface energies of 6H–SiC ($10\bar{1}0$) (case I, case II, and case III) are firstly studied and the surface calculation results show that case II and case III are more stable than case I. Then, the adhesion energies, fracture toughness values, interfacial energies, densities of states, and electronic structures of Si (220)/6H–SiC ($10\bar{1}0$) interfaces for three stacking models (AM, BM, and CM) are calculated. The CM model has the highest adhesion energy and the lowest interfacial energy, suggesting that the CM is stronger and more thermodynamically stable than AM and BM. Densities of states and the total charge densities give evidence that interfacial bonding is formed at the interface and that Si–Si and Si–C are induced due to the hybridization of C-2p and Si-3p. Moreover, the Si–C is much stronger than Si–Si at the interface, implying that the contribution of the interfacial bonding mainly comes from Si–C rather than Si–Si.

Keywords: first-principles calculations, surface interface, adhesion energy

PACS: 68.35.Af, 68.35.Ja, 68.35.bg, 68.35.B– **DOI:** 10.1088/1674-1056/23/10/106802

1. Introduction

6H–SiC is not sensitive to visible or near-infrared light, which restricts the applications of 6H–SiC in visible and near-infrared optoelectronics. A promising way to solve this problem is to use a Si/SiC heterojunction,[1–3] while the substantial defects, such as dislocations and stacking faults,[3,4] deriving from a huge theoretical lattice mismatch of 20%, at the Si/6H–SiC interface will have a serious negative influence on the quality of the prepared film, leading to the failure of devices.

In recent years, Si films have been prepared on a 6H–SiC substrate using low-pressure chemical vapor deposition (LPCVD) in our laboratory. High-purity hydrogen (H_2) is used as a carrier gas and the silane (SiH_4) is the gas source. Details of the growth process can be found in Ref. [1]. Si films with [111] and [220] orientations have been successfully grown on 6H–SiC (0001) substrate.[5] The structure of a Si (111)/6H–SiC (0001) interface has been revealed, according to the results of HRTEM and SAED. Furthermore, a molecular dynamics calculation has been employed to characterize and illustrate the interface structure of Si (111)/6H–SiC (0001) interface. The results show that atomic structure of the interface is 4:5 Si-to-SiC atomic matching.[6] Recently, the structure of a Si (220)/6H–SiC (0001) interface has also been observed.[5] The SAED patterns confirm that the parallel-plane relationship of Si/6H–SiC heterojunction is Si (220)//6H–SiC (0001) and Si (002) //6H–SiC ($10\bar{1}0$). Corresponding to the observed interface structure, the atomic structure and binding properties of Si (220)/6H–SiC (0001) interface have been simulated.[7]

As is well known, the crystal orientation of 6H–SiC substructure has a great influence on Si/SiC interface. In the low index crystal-planes of 6H–SiC, 6H–SiC ($10\bar{1}0$) can match well with Si (220), forming another possible interface model. Because of the lattice mismatch, other combinations cannot constitute a matching interface. Therefore, in this work the atomic structure and binding properties of Si (220)/6H–SiC ($10\bar{1}0$) interface are simulated and compared with those of Si (111)/6H–SiC (0001) and Si (220)/6H–SiC (0001) interfaces. It is confirmed that the Si (220)/6H–SiC ($10\bar{1}0$) is also the suitable growth model, which provides some theoretical basis for the experiment.

2. Method

Density functional theory (DFT) calculations are conducted to investigate the surface[8,9] and interface properties by using the Cambridge Sequential Total Energy Package.[10] The electron–ion interaction is described using the pseudopotential.[11,12] The generalized gradient approximation (GGA) of Perdew and Wang (PW91)[13] is employed to describe the exchange–correlation functional. The GGA potentials, representing a more inhomogeneous chemical environment, are better for the interface calculations.[14,15] The single-particle Kohn–Sham wave functions are expanded us-

*Project supported by the National Natural Science Foundation of China (Grant Nos. 61076011 and 51177134).
†Corresponding author. E-mail: hmjmm@163.com
© 2014 Chinese Physical Society and IOP Publishing Ltd

ing plane waves with a cutoff energy of 380 eV for a bulk, a surface, and an interface. A vacuum region of 10 Å is embedded into the surface and interface supercells to avoid unwanted interaction between the slab and its periodic images. The sampling of irreducible edge of Brillouin zone is performed with a regular Monkhorst–Pack grid[16] with $6 \times 6 \times 6$ k points for the bulk, and $6 \times 6 \times 1$ k points for the surface and interface. The stable state can be found by solving the Kohn–Sham equation[17] using the self-consistent field (SCF) procedure with an SCF convergence threshold of $2e^{-6}$ eV/atom. The Broyden–Fletcher–Goldfarb–Shanno (BFGS)[18] algorithm is used to relax to achieve the minimum total energy of the system and fulfill the geometry optimization with a convergence tolerance of $1e^{-5}$ eV/atom for energy, 0.01 eV/A for maximum force, and 0.001 A for maximum displacement. The exchange–correlation function, k-point sampling grids, and cutoff energy have a serious influence on the simulation accuracy. The calculation results of lattice constants (a and/or c), elastic constants (C_{ij}), and bulk modulus (B) of bulk Si and 6H–SiC ensure that the parameters used in the calculations are valid by comparing the calculation results with experimental results.

3. Results and discussion

3.1. Surface

The surface properties of materials, which are different from the bulk properties, are important since they have great decisive effects on the interaction between the substance and the external environment. In the cutting process of a 6H–SiC $(10\bar{1}0)$ surface, the dangling bonds are induced due to the breakage of chemical bonds, leading to the rise of system energy and the instability of the new surface formed. Figure 1 illustrates three kinds of surfaces: case I, case II, and case III, according to the top atom position of the cleave slab.

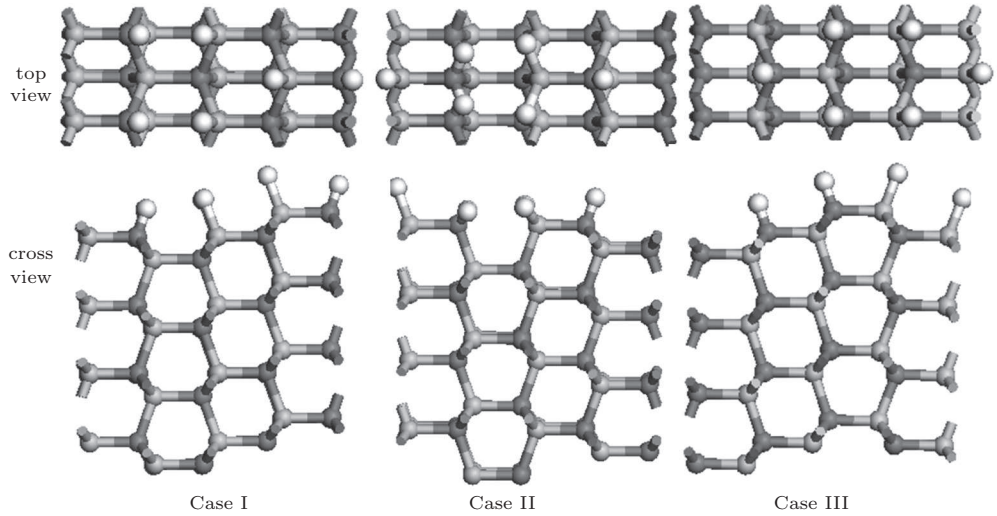


Fig. 1. Top view and cross view of three surface models (cases I–III) with three stacking sites. The spheres with colors of white, dark gray, and light gray denote H, C, and Si, respectively.

The surface energy (γ_s), which is the energy that is required to split the crystal in two parts along a plane, is the energy per unit area of the new surface formed and it can be used to describe surface stability. It can be calculated according to the following formula:[19,20]

$$\gamma_s = [E_{slab}(N) - NE_{bulk}]/(2A_s), \quad (1)$$

where $E_{slab}(N)$ denotes the total energy of surface supercell slab, E_{bulk} is the total energy per formula in the bulk material, N is the total number of formula, A_s is the surface area, and factor 2 arises from two identical surfaces of the slab.

The surface of a material is molded by a slab having a certain surface area and appropriate atom layers. Although a surface slab with more atom layers will have higher accuracy, the computation will need more memory hardware and longer computing time. In this work, the surface energy of Si (220) with ten atom layers converged well to 1.65 J/m^2 and the surface energies of case I, case II, and case III of 6H–SiC $(10\bar{1}0)$ with fifty five atom layers, are 2.961 J/m^2, 4.195 J/m^2, and 4.195 J/m^2, respectively. This implies that case I is more stable than case II and case III.

In order to clearly show the location and distribution of dangling bonds, the dangling bonds are saturated using hydrogen atoms. Consequently, the hydrogen atoms become representative of dangling bonds. The top and cross views of three kinds surfaces of 6H–SiC $(10\bar{1}0)$ are shown in Fig. 1. The number of dangling bonds is an important factor affecting surface energy bonds. Generally speaking, a bigger number of

dangling bonds is associated with a higher surface energy. It can be seen from the top view in Fig. 1 that all the three cases have six dangling bonds, so the number of dangling bonds could not be the key factor affecting surface energy. The distribution and provider of dangling bonds, observed from Fig. 1, are different for the three cases, leading to the distinctions of surface energy.

3.1.1. Interface construction

Firstly, Si (220) and 6H–Si(C) $(10\bar{1}0)$ surfaces are cleaved from the optimized bulk Si and 6H–SiC respectively. The in-plane lattice constants of Si (220) with u_{si} of 5.3 Å and v_{si} of 3.8 Å, are mismatching with those of 6H–SiC $(10\bar{1}0)$ (u_{sic} of 10.1 Å and v_{sic} of 3.8 Å). The interface properties are inherently affected by the lattice mismatch between u and v. The ratio of in-plane lattice constant of Si to that of SiC is 1–2 for u and 5–4 for v, so a 2×4 Si (220) supercell and a 1×5 6H–SiC $(10\bar{1}0)$ supercell are used to relax to the interface and minimize the system errors due to the small lattice mismatch between the two supercells. The 2×4 Si (220) supercell is stacked on a 1×5 6H–SiC $(10\bar{1}0)$ supercell to form the interface model. Considering the three different surface models of 6H–SiC $(10\bar{1}0)$, showing the distinctive surface properties as discussed above, three stacking interfacial models, called AM, BM, and CM, will be studied, which are shown in Fig. 2 in this work.

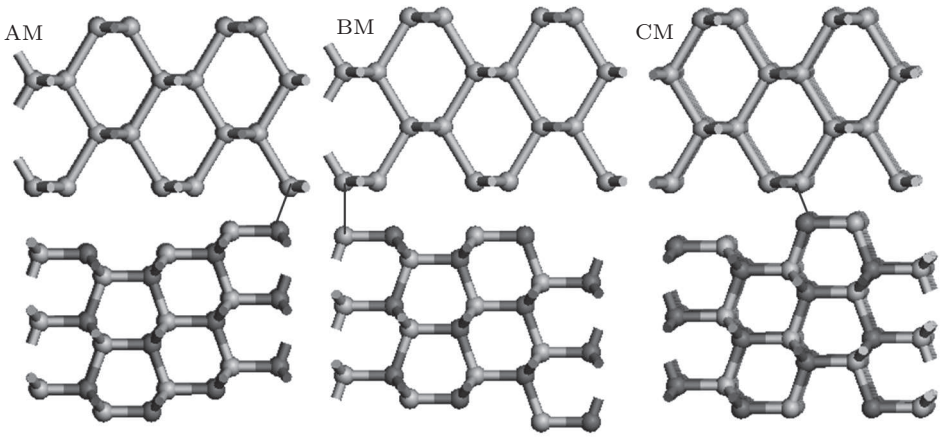


Fig. 2. Three interfacial models (AM, BM, and CM) with three stacking sites. The spheres with colors of dark gray and light gray denote C and Si, respectively.

Appropriate interfacial separations of original models will help us to create reasonable interface models and shorten the computing time. Interfacial separations of three original models are tested by energy calculation. The interfacial separations are marked using the black line in Fig. 2. The functional relationship between energy and interfacial separation is shown in Fig. 3.

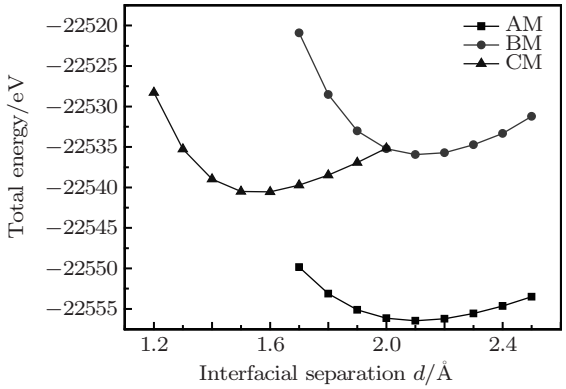


Fig. 3. Curves of total energy versus interfacial separation for the three Si (220)/6H–SiC $(10\bar{1}0)$ interface models.

Figure 3 shows that each original model has a minimum, which is representative of the most stable state, and the corresponding interfacial separation is the most appropriate interfacial separation. The most appropriate interfacial separation is 2.1 Å for AM and BM, and 1.6 Å for CM. Interface models with the proper interfacial separations are created and will relax to derive other properties.

3.1.2. Adhesion energy

Adhesion energy (W_{ad}), which is a direct measure of the interface bond strength and the work required to reversibly separate the interface into two free surfaces, is a good quantity in predicting the stability of a Si (220)/6H–SiC $(10\bar{1}0)$ interface. It can be calculated according to the following formula:[19–21]

$$W_{ad} = (E_{slab,Si\ (220)} + E_{slab,SiC\ (100)} - E_{Si\ (220)/6H-SiC\ (100)})/A, \quad (2)$$

where $E_{Si\ (220)/6H-SiC\ (100)}$ is the total energy of Si (220)/6H–SiC $(10\bar{1}0)$ interface system, and $E_{slab,Si\ (220)}$ and

$E_{\text{slab,6H-SiC (100)}}$ are the isolated Si (220) and 6H–SiC ($10\bar{1}0$) slabs in the same supercells where one slab is kept and the other is replaced by vacuum, and A is the interface area.

Interfacial fracture toughness, which describes the ability for a material to contain a crack to resist fracture, is a critical parameter in assessing the quality and performance of a Si (220)/6H–SiC ($10\bar{1}0$) interface system. According to Chen and Bielawski,[22] the interfacial fracture toughness K_{ic} along crystal orientation can be calculated from the following formula:

$$K_{\text{ic}} = 2\sqrt{W_{\text{ad}} Y_{hkl}}, \tag{3}$$

where W_{ad} is the adhesion energy, and Y_{hkl} is the Young's modulus of bulk materials along a specific crystal orientation.

Separation distance (d), which is the shortest bond length of interface models, is calculated to obtain the optimal interfacial separation. Then, the interface models with the optimal interfacial separation are relaxed. The separation distance and adhesion energy before and after relaxation for three interface models are shown in Table 1.

Table 1. Values of adhesion energy (W_{ad}) (J/m^2) and separation distance (d) (Å) of three Si (220)/6H–SiC ($10\bar{1}0$) models.

	AM	BM	CM		AM	BM	CM
$W_{\text{ad(unrelaxed)}}$	1.189	1.137	1.372	$d_{\text{opt(unrelaxed)}}$	2.1	2.1	1.6
$W_{\text{ad(relaxed)}}$	2.607	2.4859	3.849	$d_{\text{opt(relaxed)}}$	1.936	2.381	1.809
ΔW	1.418	1.3489	2.47	Δd	0.164	0.281	0.209

The fully relaxed results can be treated as the equilibrium values of three models. Relaxation has a direct influence on separation distance and adhesion energy. After relaxation, the adhesion energies are bigger than before, resulting in the more stable interfacial bonding by a possible atomic reconstruction via relaxation. The large Δd, which shows that there is a lot of change in atomic position at the Si (220)/6H–SiC ($10\bar{1}0$) interface, implies a large relaxation effect.

Separation distance and adhesion energy are also affected by stacking site. The CM has the larger W_{ad} than the other two. The W_{ad} increases as the orders of BM, AM, and CM increase, while the d increases as the opposite order increases, which confirms that the values of W_{ad} for three models are consistent with each other. Overall, the relative position of interfacial atoms has a great influence on the adhesion energy. The reason for this is that for CM, many interfacial Si atoms of Si slab interact with only one top-sited C atom or Si in SiC slab, but for AM and BM, many interfacial Si atoms of Si slab interact with C bridge-site atoms and Si atoms in SiC slab. So the bond strength of CM is stronger than those of BM and AM.

According to previous investigation, an Si-terminated Si (111)/6H–SiC (0001) interface system has a higher adhesion energy (3.4 J/m^2) than C-terminated interface (2.4 J/m^2) after relaxation, deducing that the atomic interaction at Si-terminated interface is much stronger than C-terminated interface. While for the case of the Si (220)/6H–SiC (0001) interface system, the Si-terminated interfacial adhesion energy (3.4 J/m^2) is smaller than C-terminated interface adhesion energy (4.07/m^2). So the bond strength of CM is weaker than that of C-terminated Si (220)/6H–SiC (0001), but larger than those of other interface systems.

The orientation-dependent interfacial fracture toughness can be calculated according to the above equation. The interfacial fracture toughness value is affected by adhesion energy (W_{ad}) and Young's modulus (Y_{hkl}). Young's modulus is an orientation-dependent quantity, but the three models have the same orientation and the Young's modulus can be treated as a constant. So, the W_{ad} will play an important role in determining the interfacial fracture toughness value. Interfacial fracture toughness K_{ic} should be sequenced as CM > AM > BM, according to the order of adhesion energy. That is to say, the CM has a larger interfacial fracture toughness value than the other two.

3.1.3. Interface energy

Another important quantity associated with interface thermodynamic stability is interface energy, which can be defined as the work required to form the interface from bulk material. Interface energy originates from the changes in the interfacial atomic chemical bonding and the structure strain. In contrast to the adhesion energy, it is not an absolute measure of the interface bond strength. Instead, it compares the interfacial bonds with the bonding in the bulk material, and it is calculated from the following formula:[23,24]

$$\gamma_{\text{int}} = \frac{E_{\text{si/sic}}(M,N) - ME_{\text{si}}^{\text{bulk}} - NE_{\text{sic}}^{\text{bulk}}}{A_{\text{int}}} - \gamma_{\text{si}} - \gamma_{\text{sic}}, \tag{4}$$

where $E_{\text{si}}^{\text{bulk}}$ and $E_{\text{sic}}^{\text{bulk}}$ denote the total energies of bulk Si and bulk SiC per formula, $E_{\text{si/sic}}(M,N)$ denotes the total energy of interface, M and N are the numbers of formula, γ_{si} and γ_{sic} are the surface energies, A_{int} is the interface area.

The relaxed interface energies of AM, BM, and CM, according to Eq. (4), are derived and listed in Table 2.

Table 2. Values of interface energy (γ_{int}) of three Si (220)/6H–SiC ($10\bar{1}0$) models (J/m^2).

	AM	BM	CM
γ_{int}	2.03	2.035	1.875

In the relaxation effect the relaxed interfaces are more stable than the unrelaxed interface. It can be seen from Table 2 that interfacial atomic configuration plays an important role in determining interface energy. It can be shown that the interface energies of the three interface models are very large and positive, which results from interfacial misfit strain caused by the structure mismatch of Si and SiC. If both materials are similar, then the interface energy will be very small. The sequence of interface energy of three interface models can be queued as BM(2.035) > AM(2.03) > CM(1.875). The fact that the CM has a lower value of the interface energy than AM and BM implies that CM is energetic and more favorable for the formation of an interface. The interface energy also has a relationship with the adhesion energy. It can be seen that the smaller interface energy will bring in the larger adhesion energy.

3.2. Electronic structure and bonding nature

3.2.1. Densities of states

In order to gain further an insight into the electronic states, the total densities of states (DOSs) and densities of states projected on selected atomic layers are shown in Fig. 4.

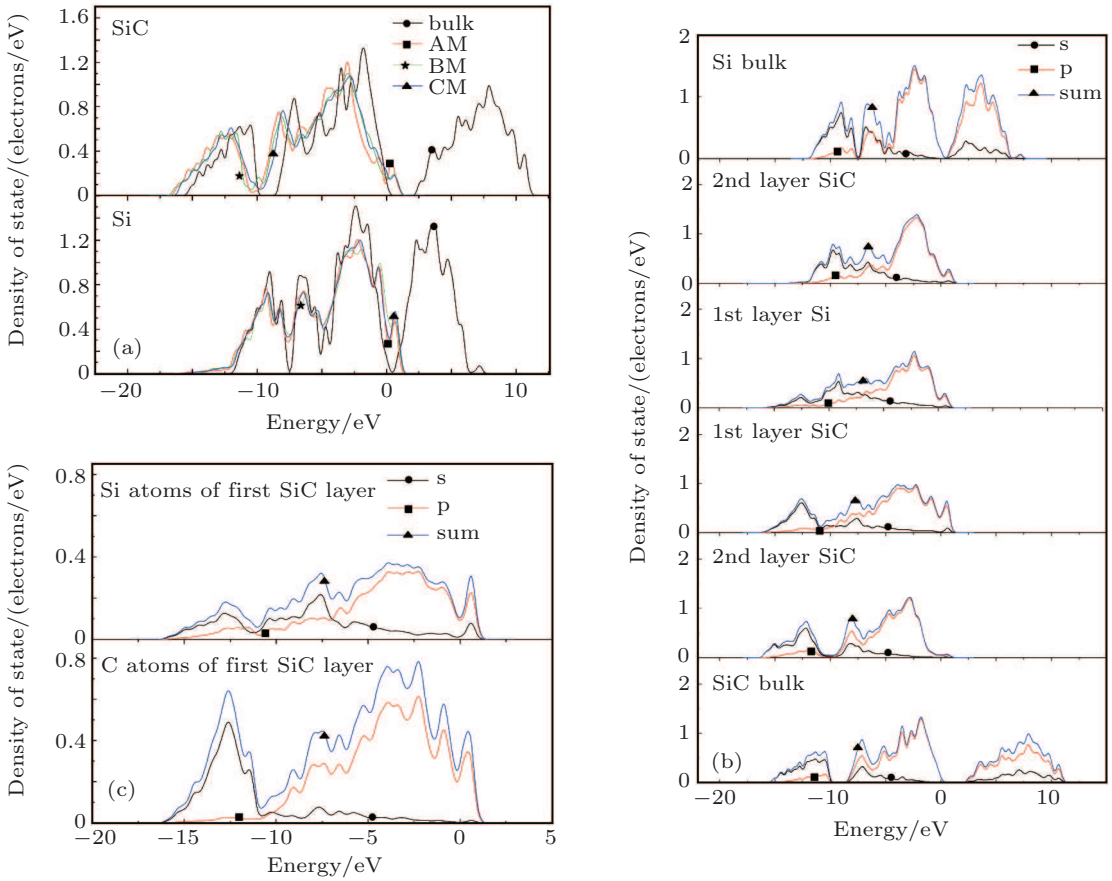


Fig. 4. (color online) (a) total DOSs of SiC and Si for bulk AM, BM, and CM, (b) DOSs projected on selected atomic layers of Si (220)/6H–SiC ($10\bar{1}0$) for CM, (c) DOSs of C atoms and Si atoms of first SiC layer for CM. The 0 eV indicates the location of Fermi level.

Figure 4(a) shows the total DOSs for Si and SiC at the interface and in pure bulk. It can be found that the DOSs from the interface is more localized than that from pure bulk, implying that stronger covalent bonding is formed because of the formation of the interface. Another noticeable feature is that a slight shift in DOS, which is induced due to the rearrangement of atoms after relaxation, occurs at the interface from the pure bulk Si and SiC. The third feature found from Fig. 4(a) is that there are new peaks around −1 eV and at 0.4 eV. The 0.4-eV peak, called interfacial state, which stems from the dangling bonds, is located at bandpap. The positions of the interfacial states of the three stacking sites are nearly the same, implying

that the stacking site has little effect on the interfacial state.

To further comprehend the advent of the new peaks, a thorough study on DOSs projected on selected atomic layers is required. Figure 4(b) reveals that the new peaks coming from the first Si layer at Si slab, ranging from −16 eV–12 eV, do not appear at the second Si layer or at bulk Si, but occur at the first SiC layer. It can also be found that there is a new peak around −1 eV at the first and second Si layer, which corresponds to the peaks at the same position at first and second SiC layer, respectively. The resonance and the overlapping states originate from the hybridization of C and Si, which mainly come from C-2p and Si-3p, confirming the existence of Si–C and Si–Si bonds. In order to measure the amount of contribution to the interfacial bonding, DOSs of C atoms and DOSs of Si atoms of first SiC layer are calculated as shown in Fig. 4(c). It can be seen from Fig. 4(c) that the DOSs of C atoms near the Fermi level are more localized than those of Si atoms, suggesting that the Si–C is much stronger than Si–Si at the interface. That is to say, the contribution of the interfacial bonding comes mainly from Si–C rather than Si–Si bonds.

3.2.2. Charge density

To identify bonding type directly, the total charge densities for three relaxed interfaces are shown in Fig. 5.

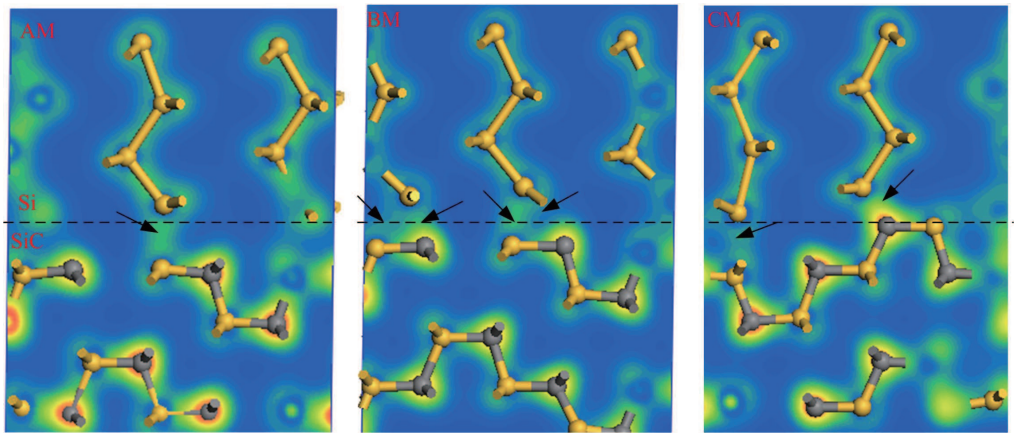


Fig. 5. (color online) Total valence electron densities of three interfacial models (AM, BM, and CM).

It can be seen from Fig. 5 that high density of charges with a saddle-shape contour can be observed along the bond axis of Si atom of Si crystal and Si atom of SiC crystal and charges are redistributed symmetrically, which indicates evidence of a non-polar Si–Si covalent bond, while the charges along the bond axis of Si atom of Si crystal and C atom of SiC crystal are redistributed asymmetrically, which is indicative of a polar Si–C covalent bond. The difference between Si–Si bond and Si–C bond is consistent with the difference in electronegativity.

Figure 5 also shows that some interfacial Si atoms in Si slab interact with an interfacial Si or an interfacial C atom in SiC slab, some interact with an interfacial Si atom and an interfacial C atom in SiC slab, and the remaining ones do not interact with the interfacial Si atoms or with the C atoms in the SiC slab. If the interfacial Si atoms of Si slab are on the top of interfacial Si atoms or C atoms of SiC slab, and the distance of the atoms is appropriate, no matter whether the two atoms will bond, then the two atoms will not interact with each other, and if the interfacial Si atoms are on the bridge sites of interfacial Si atoms and C atoms, then the Si atoms will interact with Si atoms and C atom, simultaneously.

4. Conclusions

6H–SiC $(10\bar{1}0)$ surfaces and Si (220)/6H–SiC $(10\bar{1}0)$ interfaces are calculated using the first-principles density functional theory. Three kinds of surfaces and interfaces are investigated in this work, according to the stacking sites. The surface calculation results of case I, case II, and case III show that case II and case III are more stable than case I. The adhesion energies, fracture toughness values, interfacial energies, densities of states, and electronic structures of AM, BM, and CM are calculated. From the point of view of adhesion energy, the CM has a larger value than AM and BM, suggesting that the CM is stronger and more thermodynamically stable than AM and BM. Interfacial fracture toughness is also calculated. The result indicates that the CM also has the largest value because the interfacial fracture toughness is mainly affected by adhesion energy. The interfacial energies are positive and large, which results from interfacial misfit strain caused by the struc-

ture mismatch of Si and SiC. The adhesion energy has some certain relationship with interfacial energy. For Si (220)/6H–SiC $(10\bar{1}0)$ interfaces, a smaller interface energy corresponds to a larger adhesion energy. Total DOSs, DOSs projected on selected atomic layers, and the total charge density at the interface of CM are also analyzed. The result shows that new peaks around -1 eV and at 0.4 eV are induced, implying that the interfacial bonding is formed at the interface. Si–Si and Si–C, formed at the interface, are induced due to the hybridization of C-2p and Si-3p. Moreover, the DOSs of C atoms near Fermi level are more localized than those of Si atoms, suggesting that Si–C interaction is much stronger than the Si–Si bonding at the interface.[25]

References

[1] Zhu F, Chen Z M and Li L B 2009 *Chin. Phys. B* **18** 4966
[2] Zang Y, Chen Z M, Li L B and Zhao S F 2009 *IEEE International Conference on Electron Devices and Solid-State Circuits* pp. 306–309
[3] Li L B, Chen Z M and Yang Y 2011 *Mater. Lett.* **65** 1257
[4] Li L B, Chen Z M and Xie L F 2013 *Mater. Lett.* **93** 330
[5] Xie L F, Chen Z M, Li L B, Yang C, He X M and Ye N 2012 *Appl. Surf. Sci.* **261** 88
[6] Yang C, Chen Z M and Li L B 2012 *Solid State Commun.* **152** 68
[7] Fan S J, Chen Z M, He X M and Li L B 2014 *Solid State Commun.* **177** 20
[8] Yao H and Che J G 2000 *Acta Phys. Sin.* **49** 1747 (in Chinese)
[9] Tang M S, Ma B X, Yao Q K and Jia Y 2002 *Chin. Phys.* **11** 58
[10] Payne M C, Teter M P and Allan D C 1992 *Rev. Mod. Phys.* **64** 1045
[11] Vanderbilt D 1990 *Phys. Rev. B* **41** 7892
[12] Laasonen K, Pasquarello A, Car R, Lee C, Vanderbilt D and Car-Parrinello 1993 *Phys. Rev. B* **47** 10142
[13] Perdew J P and Wang Y 1992 *Phys. Rev. B* **45** 13244
[14] Jomard G, Petit T and Pasturel A 1999 *Phys. Rev. B* **59** 4044
[15] Christensen A and Carter E A 1998 *Phys. Rev. B* **58** 8050
[16] Monkhorst H J and Pack J D 1976 *Phys. Rev. B* **13** 5188
[17] Kohn W and L J 1965 *Phys. Rev.* **140** A1133
[18] Fischer T H and Almlof J 1992 *J. Phys. Chem.* **96** 9768
[19] Abdelkader H S and Faraoun H I 2011 *J. Mater. Sci.* **50** 880
[20] Sigumonrong D P, Music D and Schneider J M 2011 *Comput. Mater. Sci.* **50** 1197
[21] Yin D, Peng X and Qin Y 2010 *J. Appl. Phys.* **108** 033714
[22] Chen K and Bielawski M 2008 *Surf. Coat. Technol.* **203** 598
[23] Lu S, Hu Q M and Yang R 2010 *Phys. Rev. B* **82** 195103
[24] Lee S J, Lee Y K and Soon A 2012 *Appl. Surf. Sci.* **25** 89977
[25] Tang C, Meng L J, Sun L Z, Zhang K W and Zhong J X 2008 *J. Appl. Phys.* **104** 113536